THE JOURNAL OF PHYSICAL CHEMISTRY Letters

Letter

pubs.acs.org/JPCL

Methylammonium Lead Bromide Perovskite Battery Anodes Reversibly Host High Li-Ion Concentrations

Nuria Vicente and Germà Garcia-Belmonte*

Institute of Advanced Materials (INAM), Universitat Jaume I, 12006 Castelló, Spain

Supporting Information

ABSTRACT: Ions migrate through the hybrid halide perovskite lattice, allowing for a variety of electrochemical applications as perovskite-based electrodes for batteries. It is still unknown how extrinsic defects such as lithium ions interact with the hybrid perovskite structure during the charging process. It is shown here that Li^+ intake/release proceeds by topotactic insertion into the hybrid perovskite host, without drastic structural alterations or rearrangement. Even the perovskite electronic band structure remains basically unaltered upon cycling. The occurrence of conversion or alloying reactions producing metallic lead is discarded. Stable specific capacity ~200 mA h g^{-1} is delivered, which entails outstanding Li-ion molar concentration, x in $Li_xCH_3NH_3PbBr_3$, approaching 3. Slight distortions of the perovskite lattice upon cycling explain the highly reversible Li^+ intercalation reaction that also exhibits an excellent rate capability.

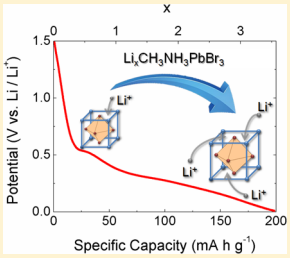

Hybrid perovskites have emerged as a family of multifunctional materials with applications in photovoltaics,[1,2] optoelectronics,[3−5] lasers,[6,7] and electrochromism.[8] Besides the interesting electronic and photonic properties exhibited by hybrid perovskites, ionic migration allows for a variety of applications in electrochemical devices. Ion transport within the lattice of perovskite compounds has applications in solid-oxide fuel cells and oxygen permeation membranes.[9,10] It is also known that hybrid perovskites behave as charge-storage materials for lithium-ion battery anodes.[11] In addition, native defects in hybrid lead halide perovskite materials are able to migrate within the perovskite structure because of the soft character of the compounds.[12] Despite the relevance extrinsic ion reaction with hybrid perovskites might have on their potential use in electrochemical devices, only a few works have addressed that issue.[11] How lithium ions interact with the hybrid perovskite structure during the charging process is still an open question.[13] It is revealed here that perovskite-based electrodes exhibit high stability upon electrochemical cycling without severe distortions of the crystal structure. This fact indicates a topotactic intercalation for Li^+ storage into the perovskite host, without drastic structural alterations or rearrangement. Lithiation proceeds in such a way that several Li ions are hosted within the same unit cell of the crystal lattice ($Li_xCH_3NH_3PbBr_3$), with x approaching 3. Moreover, the occurrence of conversion or alloying reactions producing metallic lead can be discarded.

In the present work, the hybrid perovskite $CH_3NH_3PbBr_3$ has been utilized as active material for the anode electrodes. Its interest in energy storage is related to their 3D framework of corner-connected MX_6 (M = Pb, X = Br) octahedrons with organic methylammonium cations located between them (Figure 1d). The hybrid halide perovskite AMX_3 can be then regarded as a compact structure in which the dimensionality of Li^+ transport is 3D, similarly to that occurring for spinels such as $LiMn_2O_4$, in contrast with low-dimension insertion compounds. We present here promising preliminary results and progress into the understanding of the electrochemical charging of nanostructured lead halide perovskite materials, which exhibit rather stable specific capacity ~200 mA h g^{-1} with an excellent reversibility. Rate capability between 1 and 0.25 C charging rates does not significantly change, enabling high-power performance. Although exhibiting similar electrochemical response, the issue of the underlying intercalation mechanism is not addressed by the previous works on perovskite-based anodes.[11]

Starting material was synthesized by slow evaporation of *N*,*N*-dimethylformamide (DMF, Sigma-Aldrich) in a solution containing stoichiometric amounts of lead bromide ($PbBr_2$, TCI) and methylammonium bromide (CH_3NH_3Br, > 98% TCI) 1 M in DMF. First, $PbBr_2$ and CH_3NH_3Br were dissolved in DMF; then, the solution was heated to 90 °C in magnetic stirring in a close bottle for 12 h. Solid precipitated was orange at the end of the reaction. The solution was stirred with a spatula to ensure the evaporation process of trapped solvent. Finally, it was taken out and cooled to room temperature naturally. To confirm the pure perovskite crystallographic phase, we employed a Bruker AXS-D4 Endeavor Advance X-ray diffractometer using Cu Kα, wavelength λ = 1.5406 Å.

To fabricate the working electrode, the homogeneous slurry was prepared by mixing $CH_3NH_3PbBr_3$, conductive carbon black (Super P), and poly(vinylidenedifluoride) binder (PVDF, Sigma-Aldrich) with a 80:10:10 weight ratio, respectively, by using *N*-methyl-2-pyrrolidone (NMP) as solvent. The slurry was coated on a copper foil by doctor blade and dried at 100 °C overnight. Composite electrode slices with a diameter of 10

Received: January 25, 2017
Accepted: March 10, 2017
Published: March 13, 2017

DOI: 10.1021/acs.jpclett.7b00189
J. Phys. Chem. Lett. 2017, 8, 1371−1374

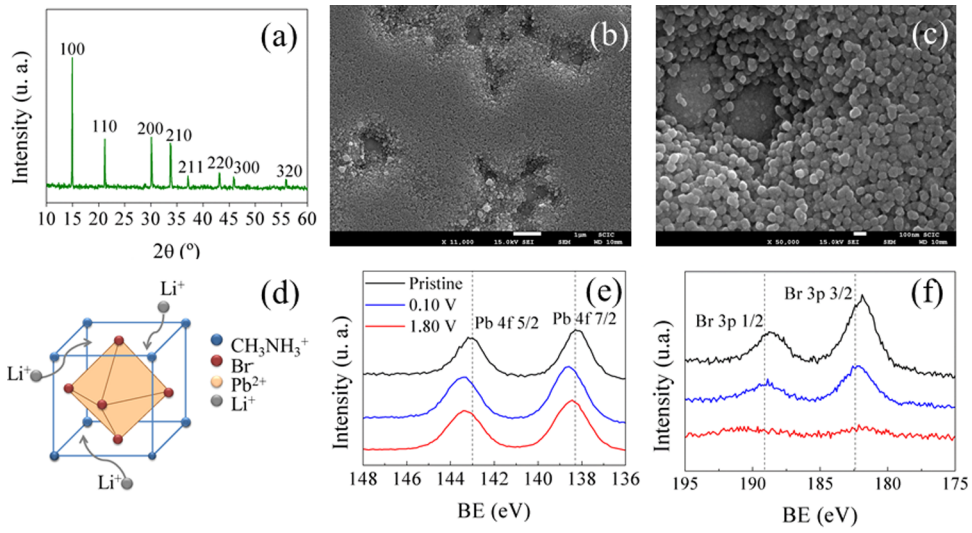

Figure 1. Structural analysis of lead bromide perovskite. (a) X-ray diffraction patterns of $CH_3NH_3PbBr_3$ powder, which can be indexed as cubic perovskite (space group = *Pm*-3m, *a* = 5.9394 Å. SEM morphology images of the $CH_3NH_3PbBr_3$ electrodes. Scale bar: (b) 1 μm and (c) 100 nm. Average perovskite particle size 65 nm. (d) Schematic crystal structure of organometal halide perovskite $CH_3NH_3PbBr_3$ indicating multiple Li-ion intake (e) Pb 4f and (f) Br 3d core-level XPS signal of $CH_3NH_3PbBr_3$ anodes at different states: pristine, 0.10 V (discharge), and 1.80 V (subsequent charge).

mm were cut and used as working electrodes for structural investigation and electrochemical analysis.

To investigate the lithium storage performance of the anode under study, a two-electrode Swagelok cell-type was used. Li metal foil was used as the counter and reference electrode, and an electrolyte-soaked microporous monolayer membrane (Celgard 2500) was employed as separator. The electrolyte is 1 M of hexafluorophosphate lithium salt ($LiPF_6$, Sigma-Aldrich) dissolved in ethylene carbonate, ethyl-methyl carbonate, and dimethyl carbonate (EC/EMC/DMC, Sigma-Aldrich) with 1:1:1 v/v/v. Cell assembly was carried out in a N_2-filled glovebox. For electrochemical characterization, a PGSTAT-30 potentiostat from AUTOLAB was employed. Cyclic voltammetry (CV) was performed in the voltage range from 0.01 to 2.00 V with a rate of 5 mV s^{-1}. The constant current charge and discharge profiles of the battery in the voltage ranged from 0.01 to 1.80 V at different rates of 50, 100, and 200 mA g^{-1}. All of the data are normalized to the load $CH_3NH_3PbBr_3$ mass.

In Figure 1a XRD patterns of $CH_3NH_3PbBr_3$ powders fabricated by means of the procedure previously described are shown. It can be indexed as a cubic perovskite structure with *a* = 5.9394 Å (space group = *Pm*-3*m*). Diffraction peaks are assigned similarly to those appearing in previous publications.[16] It is shown in Figure 1S (Supporting Information) how diffraction peak positions remain unaltered upon lithiation−delithiation, which informs on the integrity of the structure. Recent XRD analyses on $CsPbBr_3$ films after electrochemical doping reveal slight increase in the lattice constant as a consequence of lithiation, signaling negligible structural variations.[8] Figure 1b,c shows SEM images of pristine $CH_3NH_3PbBr_3$ anodes. Most particles are regular and uniform with average size around 65 nm. The electrode surface is uniform, although some pinholes are observed, within which secondary particle agglomeration occurs. It is noted here that our synthesis produces nanometer-sized particles different from those reported in previous work,[11] which shows the formation of large micrometer-sized structures by hydrothermal methods.

With the aim of investigating the chemical stability of the lead bromide perovskite upon cycling, a detailed ex situ XPS analysis at different charging states during the first charge−discharge cycle is shown in Figure 1e,f. Samples were washed out by anhydrous dimethyl carbonate (DMC) solvent several times and dried in a vacuum chamber at 60 °C for 2 h previous XPS analysis.[14] Here two elements are analyzed: bromine and lead. XPS spectra for different samples were studied using a C peak at 285.0 eV as reference, which allows identifying the valence states of the elements in pristine and cycled electrodes. In all studied electrodes, the XPS spectrum of lead appears as Pb^{2+} (Pb 4f) in Figure 1e and exhibits two peaks attributed to Pb $4f_{7/2}$ and Pb $4f_{5/2}$ levels at binding energies (BEs) of 138.7 and 143.6 eV, respectively. This is in full agreement with values previously reported.[15,16] In no case is any signal corresponding to metallic lead (Pb^0) observed. A recent analysis of $CsPbBr_3$ large single crystals has detected the presence of Pb^0 by electrochemical lithiation but using much wider ($-5 < V < 5$ V) potential windows.[8] Our results also indicate that Pb does not react to form any kind of Li−Pb alloy. It should be noted that the increase in binding energy of the Pb 4f lines (0.3 eV) upon discharge is hardly attributed to a change in the Pb oxidation state. After delithiation, XPS peaks partially recover the initial position. Small shifts can be related to a redistribution of bond electron charges.[17] It has been recently reported that ionic accumulation in perovskite compounds produces reversible lattice swell/shrink of ∼4.4%.[18] It is then not surprising that Pb bonds will undergo slight variations upon Li^+ intake and release.

Spectra of Br 3p show the Br $3p_{3/2}$ level that has a binding energy of 182.4 eV and Br $3p_{1/2}$ level of 189.1 eV (Figure 1f), similar to those previously observed. Analysis of C 1s spectra presents two peaks (see Figure 2S, Supporting Information), at 285.0 and 290.0 eV, respectively. The peak at higher energy can be assigned to Li_2CO_3 residuals, which could be formed because of electrolyte decomposition upon cycling. Finally, in the case of O 1s, the XPS bands appear at 531.8 and 532.9 eV, which is consistent with the presence of Li_2CO_3 as a cycling byproduct. Consequently, our analysis clearly confirms the stable presence of $CH_3NH_3PbBr_3$ after electrochemical cycling, indicating that successive lithium-ion intake and release does not cause severe distortions into the perovskite crystallographic

DOI: 10.1021/acs.jpclett.7b00189
J. Phys. Chem. Lett. 2017, 8, 1371−1374

structure. Moreover, also the electronic structure remains basically unaltered. It is already known that $[PbBr_6]^{4-}$ clusters largely dictate the electronic structure near the band edge.[19] Our findings point to the permanent presence of $PbBr_6$ building blocks upon lithiation and, consequently, continuity of the basic band structure. A detailed analysis of the band positions at different intercalation states would help us on this concern.[20] Electronic changes affecting the A-site organic cation cannot be discarded. These last facts signal the occurrence of a topotactic Li^+ insertion into the perovskite lattice, without severe alterations of crystal or main band structure, and unlikely occurrence of conversion or alloying reactions.

For testing electrochemical response, perovskite-based anodes were monitored by cyclic voltammetry. Figure 2a shows the first four cycles that do not change significantly through continuous cycling. It confirms the good reversibility of the electrode material. The redox peaks related to Li^+ insertion are observed at 0.49 and 0.27 V vs Li/Li^+, and the extraction from the matrix produces two peaks in the delithiation current at 0.65 and 0.75 V vs Li/Li^+. The width of the peaks and the separation between them are related to the kinetic limitations (resistances) present in the electrode. The anodic and cathodic peaks relate to the charge−discharge voltage plateaus in the galvanostatic profiles (Figure 2c). As inferred from previous XPS analysis, ion intake proceeds without severe structural changes and explains the observed redox response. To check if the lead precursor shows electrochemical activity, $PbBr_2$ electrodes were investigated to compare them with $CH_3NH_3PbBr_3$ electrodes (Figure 2a). As observed, the redox response does take place into the perovskite lattice and not within its precursors.

Galvanostatic charge−discharge test of electrodes within the voltage range 0.01 to 1.80 V vs Li/Li^+ at different charging current rate of 50, 100, and 200 mA g^{-1} can be seen in Figure 2b. A gradual fading is seen during the first several cycles. The charge and discharge specific capacities situate around 200 mA h g^{-1}, with the Coulombic efficiency above 99%, until around 20 cycles. These specific capacity values are higher than the theoretical capacity of commercial $Li_4Ti_5O_{12}$, 175.5 mA h g^{-1}. From known values of lattice constant (a = 5.93 Å), density (3.83 g cm^{-3}), and molecular weight (478.92 g mol^{-1}) of $CH_3NH_3PbBr_3$,[21] one can readily estimate the reached Li concentration per unit cell, x in $Li_xCH_3NH_3PbBr_3$. As observed in Figure 2c, lithiation attains molar contents as high as x = 3. This is certainly an outstanding charging value in comparison with other intercalation compounds, which signals multiple unit-cell Li^+ intake. It is remarkable that the first voltage plateau at 0.5 V is reached for insertion concentrations approaching x = 1 (Figure 2c). This can be interpreted in terms of a full charging, with each unit cell hosting one Li-ion, before subsequent multiple insertion. Provided the attained high Li^+ concentration, one can expect electronic density values approaching 10^{22} cm^{-3}. This is uncommon for intercalation compounds and might indicate the intrinsic ability of hybrid perovskites of holding huge amounts of conduction-band electrons without changes of the electronic structure. Recent papers have pointed out the occurrence of electronic accumulation zones at perovskite interfaces, which also imply large electronic density values.[22]

Higher capacity is reached in the first discharge curve (~600 mA h g^{-1}), which presumably corresponds to the formation of a solid electrolyte interface (SEI) layer. Cyclability has been evaluated at 50 mA g^{-1} after initial 10 cycles (Figure 2c).

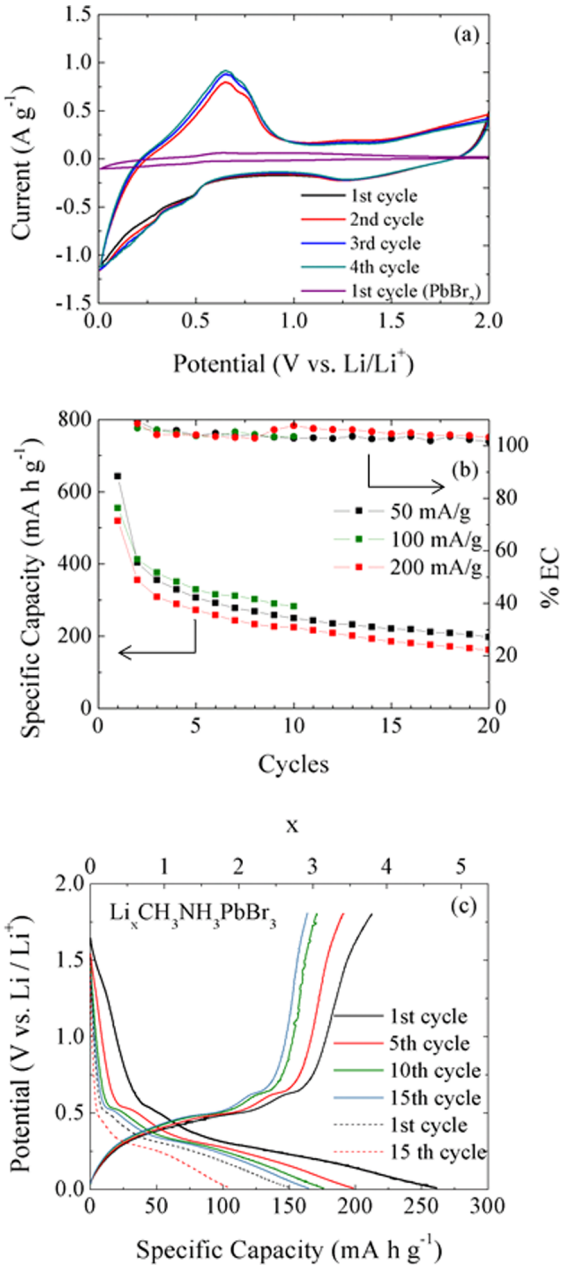

Figure 2. Battery electrochemical characterization. (a) Comparative cyclic voltammograms of $CH_3NH_3PbBr_3$ electrodes for the first four cycles in comparison with $PbBr_2$ electrode. (b) Specific capacity and Coulombic efficiency of $CH_3NH_3PbBr_3$ anodes corresponding to initial 20 cycles at different charging current densities: 50, 100, and 200 mA g^{-1}. (c) Discharge/charge voltage profiles as a function of specific capacity and corresponding Li-ion content after 10 initial cycles (continuous lines) and after 10 days of relaxation performing additional 15 cycles (dashed line).

Discharge profiles deliver specific capacities decreasing from ~265 to ~165 mA h g^{-1}. After 10 days of relaxation, an additional 15 cycles show diminution in specific capacity from 150 to 100 mA h g^{-1} (Figure 2c). As observed in Figure 2b, the rate capability does not significantly change for cycling performed between 1C and 0.25C rate charging currents (assuming 1C equaling 200 mA g^{-1}). This fact signals the occurrence of fast Li^+ intake and release presumably produced by a large value of the ionic diffusion coefficient in the lead bromide perovskite lattice.

DOI: 10.1021/acs.jpclett.7b00189
J. Phys. Chem. Lett. 2017, 8, 1371−1374

In summary, $CH_3NH_3PbBr_3$ is reported to be a promising anode material. Reversible Li^+ storage occurs by ion intercalation into the host electrode without severe distortion of the $CH_3NH_3PbBr_3$ lattice. Even the basic band structure remains unaltered for the potential window of interest. Long-term specific capacity attains significant values approaching 200 mA h g^{-1}. Lithiation reaches molar contents as high as $x = 3$ (moles of lithium per mole of methylammonium), an outstanding value in comparison with other intercalation compounds. $CH_3NH_3PbBr_3$ gathers then two main advantages: (i) it allows for high insertion concentrations with $x \gg 1$ and simultaneously (ii) it exhibits small structural distortions (topotactic intercalation). Importantly, the rate capability does not exhibit significant reduction for charging currents between 1 and 0.25C, indicating the potentiality of perovskite-based materials for high power battery applications. Our findings reveal the outstanding electronic and ionic properties of lead halide perovskites and their potential use as energy storage materials.

■ ASSOCIATED CONTENT

Supporting Information

The Supporting Information is available free of charge on the ACS Publications website at DOI: 10.1021/acs.jpclett.7b00189.

Additional XPS spectra and XRD analysis of lithiated and delithiated electrodes. (PDF)

■ AUTHOR INFORMATION

Corresponding Author

*E-mail: garciag@uji.es.

ORCID

Germà Garcia-Belmonte: 0000-0002-0172-6175

Notes

The authors declare no competing financial interest.

■ ACKNOWLEDGMENTS

We acknowledge financial support by Generalitat Valenciana under Prometeo Project (PROMETEO/2014/020) and Ministerio de Economía y Competitividad (MINECO) of Spain under Project (MAT2016-76892-C3-1-R). N.V. acknowledges University Jaume I through FPI Fellowship Program (PREDOC/2015/54). SCIC from Universitat Jaume I is also acknowledged. We acknowledge Celgard for supplying separator membranes.

■ REFERENCES

(1) Kim, H.-S.; Lee, C.-R.; Im, J.-H.; Lee, K.-B.; Moehl, T.; Marchioro, A.; Moon, S.-J.; Humphry-Baker, R.; Yum, J.-H.; Moser, J. E.; et al. Lead Iodide Perovskite Sensitized All-Solid-State Submicron Thin Film Mesoscopic Solar Cell with Efficiency Exceeding 9%. *Sci. Rep.* **2012**, *2*, 591.

(2) Liu, M.; Johnston, M. B.; Snaith, H. J. Efficient Planar Heterojunction Perovskite Solar Cells by Vapour Deposition. *Nature* **2013**, *501*, 395−398.

(3) Dou, L.; Yang, Y.; You, J.; Hong, Z.; Chang, W.-H.; Li, G.; Yang, Y. Solution-processed Hybrid Perovskite Photodetectors with High Detectivity. *Nat. Commun.* **2014**, *5*, 5404.

(4) Kim, Y.-H.; Cho, H.; Heo, J. H.; Kim, T.-S.; Myoung, N.; Lee, C.-L.; Im, S. H.; Lee, T.-W. Multicolored Organic/Inorganic Hybrid Perovskite Light-Emitting Diodes. *Adv. Mater.* **2015**, *27*, 1248.

(5) Suárez, I.; Juárez-Pérez, E. J.; Bisquert, J.; Mora-Seró, I.; Martínez-Pastor, J. P. Polymer/Perovskite Amplifying Waveguides for Active Hybrid Silicon Photonics. *Adv. Mater.* **2015**, *27*, 6157−6162.

(6) Deschler, F.; Price, M.; Pathak, S.; Klintberg, L. E.; Jarausch, D.-D.; Higler, R.; Hüttner, S.; Leijtens, T.; Stranks, S. D.; Snaith, H. J.; et al. High Photoluminescence Efficiency and Optically Pumped Lasing in Solution-Processed Mixed Halide Perovskite Semiconductors. *J. Phys. Chem. Lett.* **2014**, *5*, 1421−1426.

(7) Xing, G.; Mathews, N.; Lim, S. S.; Yantara, N.; Liu, X.; Sabba, D.; Gratzel, M.; Mhaisalkar, S.; Sum, T. C. Low-temperature Solution-processed Wavelength-tunable Perovskites for Lasing. *Nat. Mater.* **2014**, *13*, 476.

(8) Jiang, Q.; Chen, M.; Li, J.; Wang, M.; Zeng, X.; Besara, T.; Lu, J.; Xin, Y.; Shan, X.; Pan, B.; et al. Electrochemical Doping of Halide Perovskites with Ion Intercalation. *ACS Nano* **2017**, *11*, 1073−1079.

(9) Li, M.; Pietrowski, M. J.; De Souza, R. A.; Zhang, H.; Reaney, I. M.; Cook, S. N.; Kilner, J. A.; Sinclair, D. C. A Family of Oxide Ion Conductors Based on the Ferroelectric Perovskite $Na_{0.5}Bi_{0.5}TiO_3$. *Nat. Mater.* **2013**, *13*, 31−35.

(10) Mizusaki, J.; Arai, K.; Fueki, K. Ionic Conduction of the Perovskite-type Halides. *Solid State Ionics* **1983**, *11*, 203−211.

(11) Xia, H.-R.; Sun, W.-T.; Peng, L.-M. Hydrothermal Synthesis of Organometal Halide Perovskites for Li-ion Batteries. Chem. *Chem. Commun.* **2015**, *51*, 13787−13790.

(12) Unger, E. L.; Hoke, E. T.; Bailie, C. D.; Nguyen, W. H.; Bowring, A. R.; Heumüller, T.; Christoforo, M. G.; McGehee, M. D. Hysteresis and Transient Behavior in Current−Voltage Measurements of Hybrid-Perovskite Absorber Solar Cells. Energy Environ. *Energy Environ. Sci.* **2014**, *7*, 3690−3698.

(13) Zhang, W.; Eperon, G. E.; Snaith, H. J. Metal Halide Perovskites for Energy Applications. *Nat. Energy* **2016**, *1*, 16048.

(14) Haro, M.; Vicente, N.; Garcia-Belmonte, G. Oxygen Reduction Reaction Promotes Li^+ Desorption from Cathode Surface in Li-O_2 Batteries. *Adv. Mater. Interfaces* **2015**, *2*, 1500369.

(15) Schmidt, L. C.; Pertegás, A.; González-Carrero, S.; Malinkiewicz, O.; Agouram, S.; Minguez Espallargas, G.; Bolink, H. J.; Galian, R. E.; Pérez-Prieto, J. Nontemplate Synthesis of $CH_3NH_3PbBr_3$ Perovskite Nanoparticles. *J. Am. Chem. Soc.* **2014**, *136*, 850−853.

(16) Lindblad, R.; Jena, N. K.; Philippe, B.; Oscarsson, J.; Bi, D.; Lindblad, A.; Mandal, S.; Pal, B.; Sarma, D. D.; Karis, O.; et al. Electronic Structure of $CH_3NH_3PbX_3$ Perovskites: Dependence on the Halide Moiety. *J. Phys. Chem. C* **2015**, *119*, 1818−1825.

(17) Momose, H.; Honbo, H.; Takeuchi, S.; Nishimura, K.; Horiba, T.; Muranaka, Y.; Kozono, Y.; Miyadera, H. X-ray Photoelectron Spectroscopy Analyses of Lithium Intercalation and Alloying Reactions on Graphite Electrodes. *J. Power Sources* **1997**, *68*, 208−211.

(18) Zhang, Y.; Wang, Y.; Xu, Z.-Q.; Liu, J.; Song, J.; Xue, Y.; Wang, Z.; Zheng, J.; Jiang, L.; Zheng, C.; et al. Reversible Structural Swell−Shrink and Recoverable Optical Properties in Hybrid Inorganic−Organic Perovskite. *ACS Nano* **2016**, *10*, 7031−7038.

(19) Manser, J. S.; Christians, J. A.; Kamat, P. V. Intriguing Optoelectronic Properties of Metal Halide Perovskites. *Chem. Rev.* **2016**, *116*, 12956−13008.

(20) Miller, E. M.; Zhao, Y.; Mercado, C. C.; Saha, S. K.; Luther, J. M.; Zhu, K.; Stevanovic, V.; Perkins, C. L.; van de Lagemaat, J. Substrate-controlled band positions in $CH_3NH_3PbI_3$ perovskite films. *Phys. Chem. Chem. Phys.* **2014**, *16*, 22122.

(21) Weber, D. $CH_3NH_3PbX_3$, a Pb(II)-System with Cubic Perovskite Structure. *Z. Naturforsch., B: J. Chem. Sci.* **1978**, *33*, 1443−1445.

(22) Zarazua, I.; Bisquert, J.; Garcia-Belmonte, G. Light-Induced Space-Charge Accumulation Zone as Photovoltaic Mechanism in Perovskite Solar Cells. *J. Phys. Chem. Lett.* **2016**, *7*, 525−528.

DOI: 10.1021/acs.jpclett.7b00189
J. Phys. Chem. Lett. 2017, 8, 1371−1374